Asian Journal of Chemistry; Vol. 25, No. 11 (2013), 6001-6007

ASIAN JOURNAL OF CHEMISTRY

http://dx.doi.org/10.14233/ajchem.2013.14228

Heterogeneous Photocatalytic Degradation of Anionic and Cationic Dyes Over Fe-Fullerene/TiO_2 Under Visible Light

ZA-DA MENG, LEI ZHU, SHU YE, TRISHA GHOSH, KEFAYAT ULLAH, VIKRAM NIKAM and WON-CHUN OH*

Department of Advanced Materials & Science Engineering, Hanseo University, Seosan-si, Chungnam-do 356-706, South Korea

*Corresponding author: E-mail: Fax: +82 41 6883352: Tel: +82 41 6601337; E-mail: wc_oh@hanseo.ac.kr

(*Received*: 23 June 2012; *Accepted*: 22 April 2013) AJC-13388

Photocatalytic decolorization of methylene blue, methylene orange and rhodamine B in the presence of iron-treated fullerene/titania photocatalyst in aqueous solution was studied under visible light. The prepared composite photocatalyst were characterized by XRD, TEM, SEM, EDX and photocalytic activity. Its photo catalytic degradation effect was observed in the cationic dyes (methylene blue and rhodamine B) and anionic dye (methyl orange) solution. The results showed that iron incorporation enhanced the decolorization rate of dyes. The photocatalytic degradation of a dye solution could be attributed to the combined effects by the photo-degradation of titania, the synergetic effects of adsorption and photo-Fenton of Fe component. The repeatability of photocatalytic activity was also tested.

Key Words: Fullerene, TiO_2, Cationic, Anionic, TEM.

INTRODUCTION

Heterogeneous phothocatalysis has shown a high potential in applications related to liquid phase pollution control processes[1-3]. Due to the feature of using dioxygen, light and complete mineralization of organic and inorganic substrates, this method is considered as environmentally friendly for the environment pollution treatment field. Upon irradiation with light energy greater than or equal to the band gap, the electrons and holes are generated and trapped on the surface of the photocatalyst, producing reactive oxygen species such as OH and O_2 radicals to degrade organic pollutants.

Among the photocatalysts, TiO_2 has been most widely used because it is easily available, inexpensive, non-toxic, relative high chemical stability and biocompatible material that shows high photoefficiency and activity[4-7].

However, poor adsorption capacity, formation of rapid aggregates in a suspension, excitation only under UV light illumination at wavelengths below 400 nm and also recycling difficulties restricted the utilization of TiO_2. Therefore, in practical applications, attempts have been made to support TiO_2 nanoparticles on porous adsorbent materials and to extend the light absorption of the photocatalysts to the visible region[8-10]. Moreover, several researchers have already attempted to lower the band gap energy of TiO_2, which mainly includes doping with transition metal ions[11,12].

Among these materials, carbon supported TiO_2 catalysts have attracted more and more attentions. Fullerene has attracted extensive attentions for their various interesting properties due to their delocalized conjugated structures and electron-accepting ability. One of the most remarkable properties of fullerene in electron-transfer processes is that it can efficiently arouse a rapid photoinduced charge separation and a relatively slow charge recombination[13]. Thus, the combination of photocatalysts and fullerene may provide an ideal system to achieve an enhanced charge separation by photoinduced electron transfer. Some of the fullerene-donor linked molecules on an electrode exhibited excellent photovoltaic effects upon photoirradiation[14-18]. The fullerene is an *n*-type semiconductor and many organic semiconductors are *p*-type, thus by fabrication organic semiconductor/fullerene in contact, a *p-n* junction should be formed.

TiO_2 is difficult to separation from aqueous phase, so the TiO_2 powders are easy to lose and not suitable for recycling. This problem is somewhat overcome by attempts to immobilize TiO_2 on different supports, such as glass fibers, glass, quartz and stainless steel, *etc*.

Textile industries produce large volume of coloured dye effluents. Among the different types used in textile industries, 60-70 % are azo compounds. These dyes create severe environmental pollution problems by releasing toxic and potential carcinogenic substances into the aqueous phase[19].

Methylene blue is a food and drug Administration-grandfathered autoxidizable phenothiazine with potent antioxidant and metabolic enhancing properties at low doses. Methylene blue has been widely used as a supravital stain of

nervous tissue, as well as an artificial electron donor. Its major usage in pharmacotherapy is as an antidote for metabolic poisons that induce. Rhodamine B (Rh. B) and methyl orange (MO) are two important dyes which are widely used in textile industry. Rhodamine B presents strong fluorescence in aqueous solution and hence is employed as the dyeing reagent in the cell fluorescence, coloured glass and characteristic fire-cracker[20]. Methyl orange is frequently used as the pH indicator and its colour-change range is 3.1-4.4[21,22]. Although most of the dyes are not only highly toxic, they should also be recognized sufficiently by the reason of those as follows. Firstly, their colours in aqueous solution can be looked on as one sort of visual pollution. They will reduce light penetration into water due to blanching of their colours, which will decrease the efficiency of photosynthesis and affect the growth of the organisms in the water. Secondly, some dyes are easily water-soluble, it is estimated that *ca.* 20 % of dyes remains in the effluent during the production of these dyes. It was found that in photocatalytic degradation, the degradation level on unmodified TiO_2 is higher for dyes with a positive charge (cationic) than for those with a negative charge (anionic). In order to have a good photodegradation effect for not only positive charge (cationic) dyes, but also negative charge (anionic) dyes, we used Fe treated fullerene to modified TiO_2 composites to degradation these three different dyes.

In this study, the Fe-fullerene/TiO_2 composites as photocatalyst were combined to remove these three dyes: Cationic methylene blue (MB), rhodamine B (Rh. B) and anionic methyl orange (MO) from aqueous solution[23]. This study presents the preparation and characterization of Fe-fullerene/TiO_2 composites synthesized by the sol-gel method. Structural variations, surface state and photocatalytic performance were investigated, by preparing Fe-fullerene/TiO_2 and composites sequentially after oxidation, comparing to the different content of iron. X-Ray diffraction, scanning electron microscopy, energy dispersive X-ray spectroscopy and transmission electron microscope used to characterize the new complexes.

EXPERIMENTAL

Crystalline fullerene [C_{60}] powder of 99.9 % purity from TCI (Tokyo Kasei Kogyo Co. Ltd., Japan) was used as the carbon matrix. Benzene and ethyl alcohol were purchased as reagent-grade from Duksan Pure Chemical Co (Korea) and Daejung Chemical Co. (Korea) and used without further purification unless otherwise stated. Ferric nitrate [$Fe(NO_3)_3{\cdot}9H_2O$] as a iron source for the synthesis of the Fe-fullerene compounds was purchased from Duksan Pure Chemical Co. (99+%, ACS reagent, Korea). The titanium(IV) *n*-butoxide (TNB, $C_{16}H_{36}O_4Ti$) as a titanium source for the preparation of the Fe-fullerene/TiO_2 composites was purchased as reagent-grade from Acros Organics (USA). Methylene blue (MB, $C_{16}H_{18}N_3SCl{\cdot}3H_2O$) was analytical grade and also purchased from Duksan Pure Chemical Co., Ltd. Rhodamine B (Rh.B $C_{28}H_{31}N_2O_3Cl$) purchased from Samchun Pure Chemical Co., Ltd, (Korea). The methyl orange (MO, $C_{14}H_{14}N_3O_3SNa$, 99.9 %) was purchased from Daejung Chemicals & Metals Co., Ltd, (Korea).

Chemical oxidation and Fe treated: *m*-Chloroperbenzoic acid (MCPBA, *ca.* 1 g) was suspended in 50 mL benzene, followed by the addition of fullerene [C_{60}] (*ca.* 100 mg). The mixture was then refluxed in an air atmosphere and stirred for 6 h. The solvent was subsequently dried at the boiling point of benzene (353.13 K). After completion, the dark brown precipitates were washed with ethyl alcohol and dried at 323 K, after this the oxidation fullerene was formed. For iron decoration, nomenclatures of samples for the ferric nitrate solution (0.05, 0.10 and 0.50 M) were showed in Table-1. This mixture was refluxed in an air atmosphere and stirred at 343 K for 6 h using a magnetic stirrer in a vial. After being heat treatment at 773 K for 1 h, the Fe-fullerene compounds were formed.

TABLE-1
NOMENCLATURES OF SAMPLES PREPARED WITH FE-FULLERENE/TiO_2 COMPOSITES

Preparation method	Nomenclatures
MCPBA+ benzene+ C_{60} +0.05 M $Fe(NO_3)_3$ + TNB	FCT1
MCPBA+ benzene+ C_{60}+ 0.10 M $Fe(NO_3)_3$+ TNB	FCT2
MCPBA+ benzene+ C_{60}+ 0.15 M $Fe(NO_3)_3$+ TNB	FCT3

Preparation of Fe-fullerene/TiO_2 composites: Fe-fullerene was prepared using pristine concentrations of titanium(IV) *n*-butoxide for the preparation of Fe-fullerene/TiO_2 composites. Fe-fullerene powder was mixed with 3 mL titanium(IV) *n*-butoxide. Then the solutions were homogenized under reflux at 343 K for 5 h, while being stirred in a vial again. After stirred, the solution transformed into Fe-fullerene/TiO_2 gels and these gels were heat treatment at 923 K, then Fe-fullerene/TiO_2 composites were produced.

Characterization of Fe-fullerene/TiO_2 compounds: For the measurements of structural variations, XRD patterns were taken using an X-ray generator (Shimatz XD-D1, Japan) with CuK_α radiation. SEM was used to observe the surface state and structure of Fe-fullerene/TiO_2 composites using a scanning electron microscope (JSM-5200 JOEL, Japan). Energy dispersive X-ray (EDX) was also used for the elemental analysis of the samples. The specific surface area (BET) was determined by N_2 adsorption measurements at 77 K (Monosorb, USA). Transmission electron microscopy (TEM, JEOL, JEM-2010, Japan) were used to observe the surface state and structure of the Fe-fullerene/TiO_2 composites. At acceleration voltage of 200 kV, TEM was used to investigate the size and distribution of the titanium and iron particles deposit on the fullerene surface of various samples. TEM specimens were prepared by placing a few drops of the sample solution on a carbon grid. The whole experimental apparatus were shown in Fig. 1.

Photocatalytic activity measurements: A specified quantity of Fe-fullerene/TiO_2 composites was added to 50 mL methylene blue solution. The reactor was placed for 2 h in the darkness, in order to make the Fe-fullerene/TiO_2 composites particles adsorbed the methylene blue molecule maximum. The initial concentrations of the dyes were set at 1×10^{-5} mol/L in all experiments. The amount of the Fe-fullerene/TiO_2 composite was 0.05 g/(50 mL solution). After adsorption, photodecompositions of the dyes solutions were performed

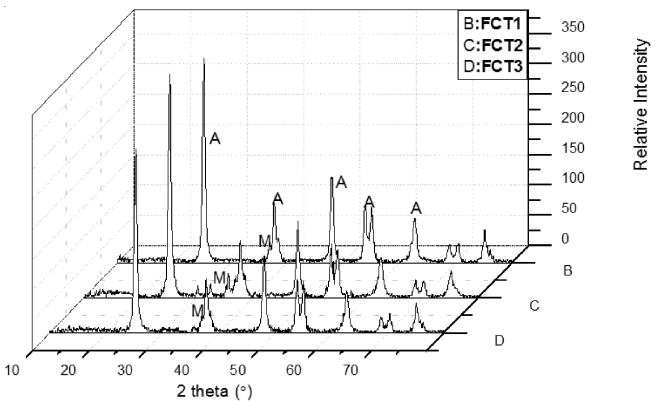

Fig. 1. XRD patterns of Fe-fullerene /TiO_2 composites

under visible light in the dark-box, so that the reactor is irradiated by a single light source. UV light irradiation of the photoreactor was done for 10, 30, 60, 90, 120 and 150 min, respectively, to research the degradation of the dyes solutions. The experiments were performed at room temperature. In the process of degradation of dyes, a glass reactor (bottom area = 20 cm^2) was used and the reactor was placed on the magnetic churn dasher. Samples were then withdrawn regularly from the reactor and removal of dispersed powders through a centrifuge. The concentration of methylene blue in the solution was determined as a function of irradiation time.

Circle use for Fe-fullerene/TiO_2 composites: The cleaned Fe-fullerene/TiO_2 composites were immersion in ethanol for 6 h and rinsed with deionized water and then dried at 353 K. After this the cleaned Fe-fullerene/TiO_2 composites were reused for remove dyes and the circle experiment is doing several times.

RESULTS AND DISCUSSION

Structural analysis: The XRD patterns of the samples prepared with the different amounts of iron are displayed in Fig. 1. 'C' is the characteristic peak corresponding to the fullerene, 'A' is anatase phase of titanium, 'F' is Fe and 'M' is Fe_2O_3. It can be seen that the diffraction peaks of all samples are ascribed to the peak of TiO_2 anatase phase whatever how much Fe was doped. The diffraction pattern peaks rerated to the anatse phase (2θ = 25.3, 37.5, 48.0, 53.8, 54.9 and 62.5) were clearly observed, which were diffractions of (101), (004), (200), (105), (211) and (204) planes of anatase[23]. It is known that three polymorphs of titania are: anatase, rutile and brookite. Among the three, anatase TiO_2 has the highest photocatalytic activity. There is no peak for the other TiO_2 phases (rutile or brookite) appear. The results also indicate that the phase transition from titanium(IV) *n*-butoxide to the anatase phase took place at 923 K, with formation of titania crystalline.

Elemental analysis: Fig. 2 shows the EDX spectra of the prepared photocatalysts compounds. Table-2 lists the results of the EDX elemental microanalysis of the photocatalysts compounds. The EDX data confirms the existence of the main elements, namely C, O, Ti and Fe, as well as other impure elements. The date also shows that most of the spectra for these samples produce stronger peaks for carbon and Ti elements than for any other elements. The peak of Fe increased with an enhancement of the dosage of $Fe(NO_3)_3$ during the process of prepare Fe-fullerene composites. There are some small impurities which are considered into the composites using the fullerene without purification. In case of the most of the samples, carbon and titanium were present as major elements with small quantities of oxygen in the composite.

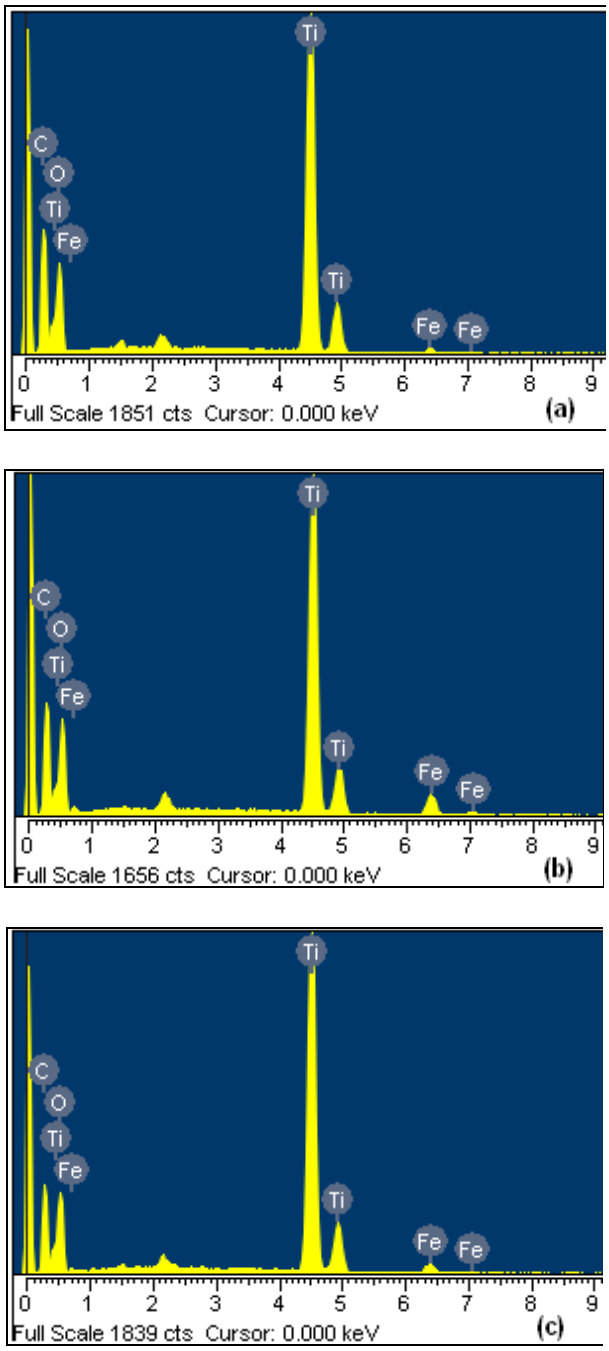

Fig. 2. EDX elemental microanalysis for Fe-fullerene/TiO_2 composite: (a) FCT1, (b) FCT2 and (c) FCT3

TABLE-2
EDX ELEMENTAL MICROANALYSIS AND BET VALUE OF Fe-FULLERENE/TiO_2 COMPOSITES

Sample name	C (wt. %)	O (wt. %)	Ti (wt. %)	Fe (wt. %)	BET (m^2/g)
FCT1	25.01	40.36	33.73	0.90	40.4
FCT2	20.12	41.00	37.08	1.80	31.3
FCT3	22.77	40.61	32.08	3.75	22.5

Surface characteristics: SEM micrographs revealed three different Fe-fullerene/TiO_2 composites derivatives with surface characteristics shown in Fig. 3. Fig. 3(a) is SEM image for FCT1, (b) is FCT2 (c) is FCT3 and Fig. 3 shows different magnification for 1000 and 2000, respectively. The TiO_2 grain structure is clearly visible with a great distribution on the surface of fullerene, may be a majority of TiO_2 attached in the 3-D matrix. As shown in Fig. 3, for the Fe-fullerene/TiO_2 composite, the morphological evidences of TiO_2 units onto Fe-fullerene structure which seem to cover the fullerene surface. These TiO_2 particles were regularly dispersed on the fullerene surfaces and continuous TiO_2 units was immobilized on almost every grain of fullerene. It is considered that a good dispersion of small particles on the fullerene surface could provide evidence for the existence of more reactive sites for photo decomposition of the dye[24]. But the large clusters with an irregular agglomerate dispersion could not found, due to the titanium(IV) *n*-butoxide (TNB, $C_{16}H_{36}O_4Ti$) as a titanium source have a low proportion.

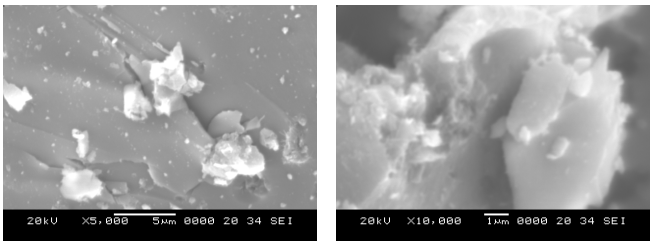

(a)

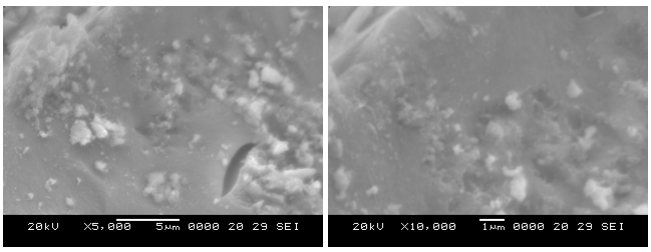

(b)

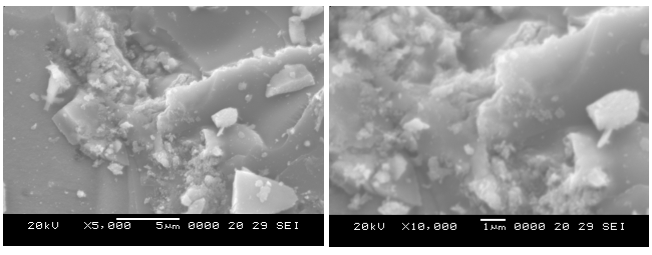

(c)

Fig. 3. SEM micrographs of Fe-fullerene/TiO_2 composites: (a) FCT1, (b) FCT2 and (c) FCT3

The values of the specific surface area (BET) are shown in Table-2. It is clearly seen that the surface area of Fe-fullerene/TiO_2 samples is decreased with an increasing amount of iron ion. The BET value is decrease from 85 of pure fullerene to 22.5 of FCT_3. It can be considered that the TiO_2 and iron was introduced into the pore of the fullerene and thus decreased the BET surface area. The sample FCT1 has the largest surface area which can affect the adsorption reaction.

The interfacial region of the Fe-fullerene/TiO_2 compound was investigated by TEM to obtain additional information about the interfacial region of the fullerene crystals and to identify potential reaction products in this domain. Fig. 4 is the TEM image for FCT1 at different measure. Fig. 4 showed that the large clusters with an irregular agglomerate dispersion of TiO_2. The fullerene particles are clearly shown from this picture. From Fig. 4(a), the iron particles have a uniform distribution in this Fe-fullerene/TiO_2 composites, this made the composites have good photodegradation efficiency and stability activity. In picture (b), fullerene and iron are based on TiO_2 particles. Compare this two TEM image, we can see that the composition of compounds particles dispersed well and very uniform.

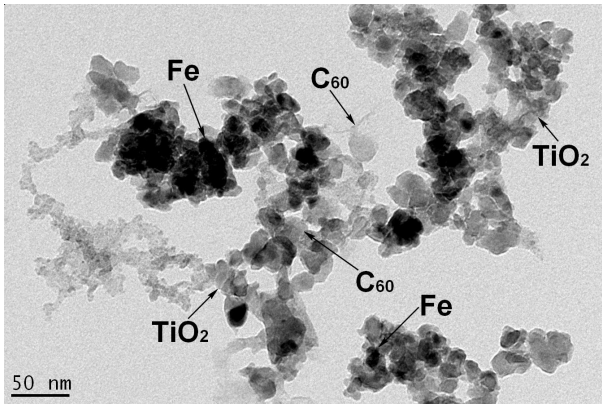

(a)

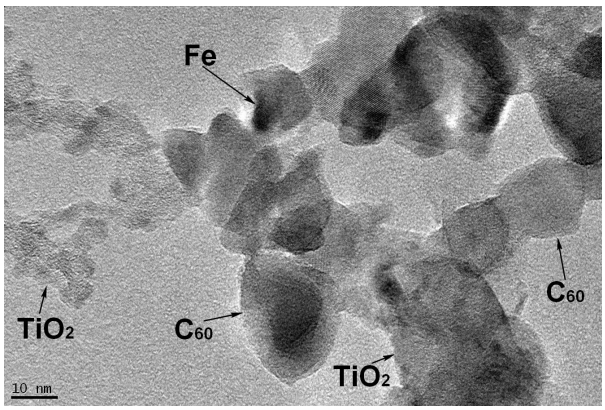

(b)

Fig. 4. TEM micrographs of Fe-fullerene/TiO_2 composites

Adsorption effect of Fe-fullerene/TiO_2: During the process of photocatalytic effect of dyes, there has two steps; first, adsorbed dye molecules and second, degradation dye molecules. Fig. 5 is the adsorptive effect of Fe-fullerene/TiO_2 for different dyes. According to Fig. 5, it can be saw that adsorptive effect of three kinds of dye molecules, methylene blue and methyl orange molecules were adsorbed more easily by Fe-fullerene/TiO_2 compounds.

For the adsorption of the adsorbates on to the adsorbent in aqueous solution, two diffusion steps are necessary: mass transfer from water to the adsorbent surface across the boundary layer and diffusion in the porous particle. It was found that the adsorption capacity of the biomass for the two dyes

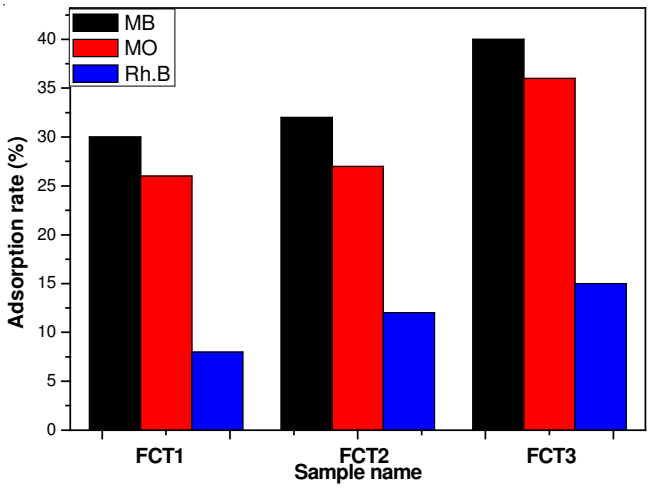

Fig. 5. Adsorption rate for Fe-fullerene/TiO_2 composites

increased with the increase of their equilibrium concentration, until maximum values were obtained. In order to investigate the adsorption model, Langmuir and Freundlich adsorption isotherms were used to fit the adsorption curves. The Langmuir and Freundlich isotherms may be expressed as eqns. 1 and 2, respectively[25-27].

$$\frac{C_e}{q_e} = \frac{1}{b} \times qm + \frac{C_e}{q_m} \quad (1)$$

$$\ln q_e = \ln a + \frac{1}{n} \ln C_e \quad (2)$$

where 'q_m' is the maximum amount of adsorption (mg g^{-1}), 'b' is the adsorption equilibrium constant (Lm g^{-1}), 'C_e' is the equilibrium concentration of substrates in the solution (mol L^{-1}), 'a' is a constant representing the adsorption capacity and 'n' is a constant depicting the adsorption intensity. According to the Langmuir equation, the maximum uptake capacities (q_m) order for methylene blue, methylene orange and rhodamine B were MB > MO > Rh. B.

For the other hands the BET specific surface area of the adsorbent, polarity matching between the adsorbent and the adsorbate, pore structure of the adsorbent and the matching of the pore size of the adsorbent with the size of the adsorbate are thought to be the main factors influencing the adsorption. If the pore diameter of the adsorbent is too small, intra-particle diffusion will be hindered, which affects the adsorption in a negative way. On the other hand, the adsorption is also not favorable if the pore diameter is too large. The BET specific surface area of the adsorbent is only important factor for adsorption effect. The polarity matching between the adsorbent and the adsorbate, pore structure of the adsorbent and the matching of the pore size of the adsorbent with the size of the adsorbate are main factors influencing the adsorption. The larger adsorption capacity is derived from good matching of the pore diameter to the molecular diameter. Table-3 shows the molecule size of MB, MO and Rh.B. There were three tropisms when a molecule was adsorbed on a sorbent; for example, for MB molecules, which obversed tropism (1.43 nm × 0.61 nm), end tropism (1.43 nm × 0.4 nm) and side tropism (0.61 nm × 0.4 nm), respectively. Because the width and height of rhodamine B molecule (1.09 and 0.64 nm) were

TABLE-3
STRUCTURAL REPRESENTATION OF ORGANIC DYES

Dyes	Molecular structure of dyes
MB λ_{max} = 660 nm	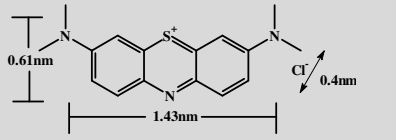
Mo λ_{max} = 476 nm	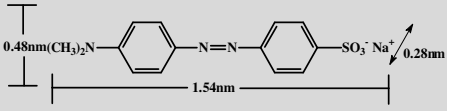
Rh.B λ_{max} = 550 nm	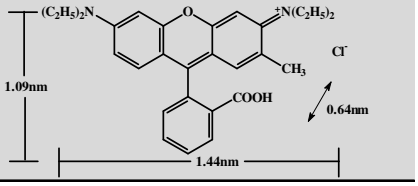

larger than methylene blue and methyl orange, these pores could absorb more methylene blue and methyl orange molecules than that of rhodamine B from obverse tropism, side tropism and end tropism[28-30]. To evaluate the actual photocatalytic activity of Fe-fullerene/TiO_2 photocatalysts compared with the decomposition processes of these three organic dyes, methylene blue was decomposed at a higher degree than that of methyl orange and rhodamine B, as shown with the curves of degradation.

Degradation effect of Fe-fullerene/TiO_2: Fig. 6 is the results of Fe-fullerene/TiO_2 photocatalysts degradation different dyes under visible light. Picture (a) is degradation of MB solution, (b) is degradation of MO solution and (c) is degradation of Rh.B solution. In picture (a), from these spectra for the MB solutions after photolysis, the relative yields of the photolysis products formed under different irradiation time conditions are shown for the products. The concentration of dye was 1.0×10^{-5} mol/L and the absorbance decreased with an increase of irradiation time. This implies that the light transparency of the dye concentration increased greatly by the photocatalytic degradation effect. An effect of the high crystallinity of the anatase phase on photocatalytic degradation of dye has been shown. As mentioned above, fullerene had an energy sensitizer for improving the quantum efficiency and an increase of charge transfer. It is believed that the degradation of dye concentration in the aqueous solution can be caused by the quantum efficiency of the Fe_2O_3-fullerene, photocatalytic decomposition by TiO_2 and decomposition of an organic reaction by the iron particles. Dye molecules absorb energy from irradiation, thereby shifting their delocalized electrons from bonding to antibonding orbitals. It is believed that the TiO_2 deposited on the fullerene surface can retain its photo-degradation activity. In the presence of adsorbed FCT molecules, photo-generated electrons are scavenged by FCT molecules (Fig. 6). The scavenged electrons ultimately enter reduction reactions, assuming that fullerenes as an electron relay similar to that suggested by Guldi and Prato[31].

Fig. 6 shows the degradation of dye solution. FCT_3 has good photocatalytic activity, due to the large content of iron, which can be seen in Fig. 3. Table-2 showed that Fe-fullerene/TiO_2 compounds have a little specific surface area, so the accumulation of glass, liquids, or solutes on the surface is poor.

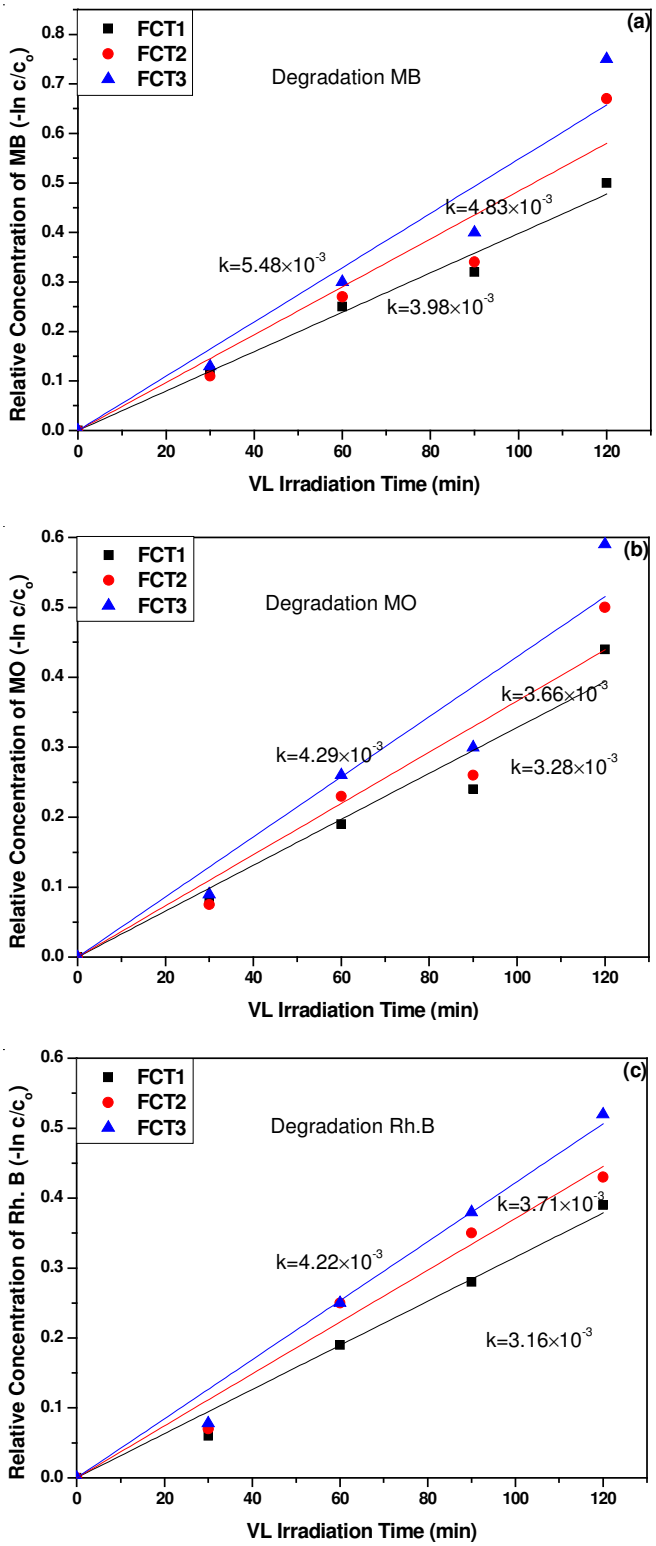

Fig. 6. Different dye solutions on time of visible light irradiation for Fe-Fullerene/TiO_2 composites: (a) MB, (b) MO, (c) Rh. B

Iron-doped, Fe^{3+} can improve the photocatalytic efficiency by enhancing processes such as separation of photogenerated charges (by hole or electron trapping), detrapping and/or transfer of trapped charges to interface and to adsorbed substrates and reducing consequently recombination[32,33].

In these compounds, fullerene is not only used for adsorbent and conductive material, but also as light-harvesting system. Light-harvesting system is able to absorb light and channel the energy. Fullerene is one of the promising materials because of its band gap energy, *ca.* 1.6-1.9 eV[34,35]. So when the Fe-fullerene/TiO_2 composites is irradiated with UV light, some electrons are promoted from the valence band *via* fullerene to the conduction band of the TiO_2 to produce electron-hole (e^- and h^+) pairs and the electron transfer between fullerene and TiO_2 can be beneficial to enhance the photocatalytic activity of the composite. Fullerene also harvesting the light to produce electron-hole (e^- and h_{vb}^+) pairs resulted in enhances the sonocatalytic activity.

$$C_{60} + h\nu \rightarrow C_{60}^{+} + e^{-} + h_{vb}^{+} \quad (3)$$

$$e^{-} + O_2 \rightarrow O_2^{\bullet} \quad (4)$$

$$h_{vb}^{+} + H_2O \rightarrow OH^{\bullet} + H^{\bullet} \quad (5)$$

Iron and fullerene can enhance the producing capacity for $OH^{\bullet}$ radicals, so Fe-fullerene/TiO_2 has the high photocatalytic activity during the photocatalytic degradation, as shown in Fig. 6.

Cycles of degradation: To evaluate the photochemical stability of the catalyst, the repeated experiments for the photodegradation of MB solutions were performed Fe-fullerene/TiO_2 samples and the results are shown in Fig. 7. As shown in Fig. 7, 54 % of MB could be degraded when FCT1 is used for the first time. However, after four recycles, a rather too decrease of photocatalytic activity for FCT1 is found and 47 % of MB is degraded within 2 h. The In contrast, as shown in Fig. 7 the reused Fe-fullerene/TiO_2 sample does not show apparent change in photocatalytic activity, which emphasizes the excellent photochemical stability of the Fe-fullerene modified photocatalyst. Fe-fullerene modification can not only improve the photocatalytic performance but also long term stability of TiO_2 nanocrystals. This result is significant from the viewpoint of practical application, as the enhanced photocatalytic activity and prevention of catalyst deactivation will lead to more cost-effective operation[36].

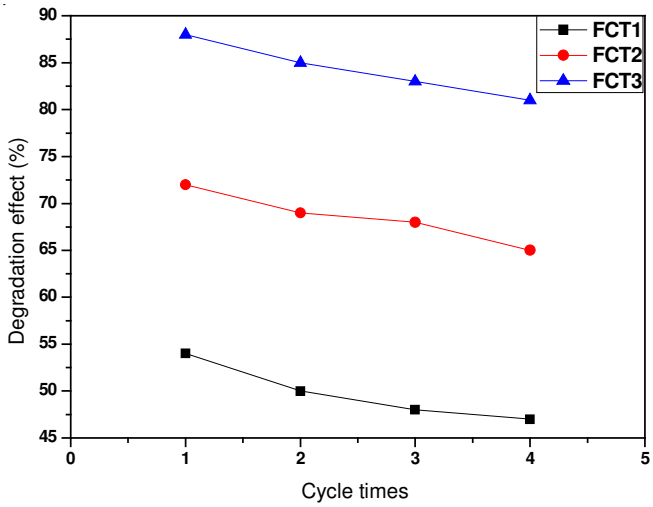

Fig. 7. Reuse experiment for Fe-fullerene/TiO_2 composites

Conclusion

In this study, we presented the preparation and characterization of Fe-fullerene/TiO_2 composites. Fe-fullerene/TiO_2

composites about different content of iron were characterized by their structural variations, surface state and photocatalytic by XRD, SEM, EDX spectroscopy and TEM. In the XRD patterns for the Fe-fullerene/TiO_2 composite, the diffraction patterns demonstrated peaks of high crystallinity of anatase. In the SEM image, TiO_2 particles regularly dispersed on the fullerene surface. The EDX spectrum showed the presence of C, O and Ti, as major elements, with strong Fe peaks. The photodegradation effects of Fe-fullerene/TiO_2 composites are great for both cationic and anionic dyes under visible light irradiate, the adsorption effect is dissimilarity because of the different pore size and different molecule size of dyes. Fe-fullerene/TiO_2 composites have the best photocatalytic activity for methylene blue solutions and also have good photocatalytic activity in cycles experiment.

REFERENCES

1. Z.D. Meng, K.Y. Cho and W.C. Oh, *Asian J. Chem.*, **23**, 847 (2011).
2. W.C. Oh, J.H. Son, F.J. Zhang and M.L. Cheng, *J. Korean Ceram. Soc*., **46**, 1 (2009).
3. W.C. Oh, A.R. Jung and W.B. Ko, *Mater. Sci. Eng*., **C29**, 1338 (2009).
4. Z.D. Meng, K. Zhang and W.C. Oh, *Korean J. Mater. Res*., **20**, 228 (2010).
5. Z.D. Meng, L. Zhu, J.G. Choi, F.J. Zhang and W.C. Oh, *J. Mater. Chem*., **21**, 7596 (2011).
6. A. Fujishima, T.N. Rao and D.A. Tryk, *J. Photochem. Photobiol*., **C1**, 1 (2000).
7. C.K. Xu, R. Killmeyer, L. Gray and M. Khan, *Appl. Catal. B*., **64**, 312 (2006).
8. M.V. Shankar, S. Anandan, N. Venkatachalam, B. Arabindoo and V. Murugesan, *Chemosphere*, **63**, 1014 (2006).
9. H.G. Yu, S.C. Lee, J. Yu and C.H. Ao, *J. Mol. Catal. A*, **246**, 206 (2006).
10. Y.M. Sung, K.S. Park, S.M. Park and G.M. Anilkumar, *J. Cryst. Growth*, **286**, 173 (2006).
11. H.J. Yun, H. Lee, J.B. Joo, N.D. Kim, M.Y. Kang and J.H. Yi, *Appl. Catal. B: Environ.*, **94**, 241 (2010).
12. C.S. Hsu, C.K. Lin, C.C. Chan, C.C. Chang and C.Y. Tsay, *Thin Solid Films*, **494**, 228 (2006).
13. S. Ito, T. Kitamura, Y. Wada and S. Yanagida, *Sol. Energy Mater. Sol. Cells*, **76**, 3 (2003).
14. J.J. Davis, H.A.O. Hill, A. Kurz, A.D. Leighton and A.Y. Safronov, *J. Elem. Chem*., **429**, 7 (1997).
15. A. Szucs, A. Loix, J.B. Nagy and L. Lamberts, *J. Elem. Chem*., **397**, 191 (1995).
16. Z.D. Meng, L. Zhu, J.G. Choi, C.Y. Park and W.C. Oh, *Nanoscale Res. Lett*., **6**, 459 (2011).
17. M.C. Buzzeo, R.G. Evans and R.G. Compton, *Chem. Phys. Chem*., **5**, 1106 (2004).
18. R.C. Haddon, A.F. Hebard, M.J. Rosseinsky, D.W. Murphy, S.J. Duclos, K.B. Lyons, B. Miller, J.M. Rosamilia, R.M. Fleming, A.R. Kortan, S.H. Glarum, A.V. Makhija, A.J. Muller, R.H. Eick, S.M. Zahurak, R. Tycko, G. Dabbagh and F.A. Thiel, *Nature*, **350**, 320 (1991).
19. J. Yu, X. Zhao and Q. Zhao, *Thin Solid Films*, **379**, 7 (2000).
20. S. Nagaoka, Y. Hamasaki, S. Ishihara, M. Nagata, K. Iio, C. Nagasawa and H. Ihara, *J. Mol. Catal. A*, **177**, 255 (2002).
21. J.C. Rojas, N. SimolA, B.A. Kermath, J.R. Kane, T. Schallert and F. Gonzalez-Lima, *Neuroscience*, **163**, 877 (2009).
22. W. Baran, A. Makowaki and W. Wardas, *Dyes Pigments*, **76**, 226 (2008).
23. D. Zhang, T. Yoshida and H. Minoura, *Adv. Mater*., **15**, 814 (2003).
24. X.W. Zhang, M.H. Zhou and L.C. Lei, *Carbon*, **43**, 1700 (2005).
25. X.Y. Jin, M.Q. Shan, Z.G. Pei and Z.L. Chen, *J. Colloid Interf. Sci*., **328**, 243 (2008).
26. A. Ayar, A. Gezici and M. Kucukosmanoglu, *J. Hazard. Meter.*, **146**, 186 (2007).
27. J.X. Yu, B.H. Li, X.M. Sun, Y. Jun and R.A. Chi, *Biochem. Eng. J*., **45**, 145 (2009).
28. S. Kundu, S.K. Ghosh, M. Mandal, T. Pal and A. Pal, *Talanta*, **58**, 935 (2002).
29. E. Haque, J.W. Jun and S.H. Jhung, *J. Hazard. Mater*., **185**, 507 (2011).
30. J.H. Huang, K.L. Huang, S.Q. Liu, A.T. Wang and C. Yan, *Colloids Surf. A*, **330**, 55 (2008).
31. D.M. Guldi and M. Prato, *Acc. Chem. Res*., **33**, 695 (2000).
32. W.Y. Choi, A. Termin and M.R. Hoffmann, *J. Phys. Chem. B*., **98**, 13669 (1994).
33. A. Kumbhar and G. Chumanov, *J. Nanoparticle Res*., **7**, 489 (2005).
34. G.K.R. Senadeera and V.P.S. Perera, *Chinese J. Phys*., **43**, 384 (2005).
35. T. Hasobe, S. Hattori, P.V. Kamat and S. Fukuzumi, *Tetrahedron*, **62**, 1937 (2006).
36. L.G. Devi, B.N. Murthy and S.G. Kumar, *Chemosphere*, **76**, 1163 (2009).